parallelity for phase imaging, single crystals should be employed after passing the x-ray beam through the polycapillary.

Since it is possible to increase the irradiation field by increasing the distance between the x-ray source and the polycapillary, this system can be applied to image a wide variety of objects in various fields, including medical radiography.

Acknowledgments

This work was supported by Grants-in-Aid for Scientific Research (13470154, 13877114, and 16591222) and Advanced Medical Scientific Research from MECSST, Grants from Keiryo Research Foundation, The Promotion and Mutual Aid Corporation for Private Schools of Japan, JST (Test of Fostering Potential), NEDO, and MHLW (HLSRG, RAMT-nano-001, RHGTEFB-genome-005, and RGCD13C-1).

References

1) Davis T J, Gao D, Gureyev T E, et al.: Phase-contrast imaging of weakly absorbing materials using hard x-rays. Nature 373: 595-597, 1995
2) Momose A, Takeda T, Itai Y, et al.: Phase-contrast x-ray computed tomography for observing biological soft tissues. Nature Medicine 2: 473-475, 1996
3) Ishisaka A, Ohara H and Honda C: A new method of analyzing edge effect in phase contrast imaging with incoherent x-rays. Opt. Rev. 7: 566-572, 2000
4) Akisada A, Ando M, Hyodo K, Hasegawa S, et al.: An attempt at coronary angiography with a large size monochromatic SR beam. Nucl. Instrum. Meth. Phys. Res. A246: 713-718, 1986
5) Thompson A C, Zeman H D, Brown G S, et al.: First operation of the medical research facility at the NSLS for coronary angiography. Rev. Sci. Instrum. 63: 625-628, 1992
6) Mori H, Hyodo K, Tanaka E, et al.: Small-vessel radiography in situ with monochromatic synchrotron radiation. Radiology 201: 173-177, 1996
7) Hyodo K, Ando M, Oku Y, et al.: Development of a two-dimensional imaging system for clinical applications of intravenous coronary angiography using intense synchrotron radiation produced by a multipole wiggler. J. Synchrotron Rad. 5: 1123-1126, 1998
8) Sato E, Komatsu M, Hayasi Y, et al.: Quasi-monochromatic parallel radiography achieved with a plane-focus x-ray tube. SPIE 4786: 151-161, 2002
9) Sato E, Sagae M, Ichimaru T, et al.: Tentative study on x-ray enhancement by fluorescent emission of radiation by plasma x-ray source. SPIE 3771: 51-60, 1999
10) Sato E, Hayasi Y, Germer R, et al.: Intense characteristic x-ray irradiation from weakly ionized linear plasma and applications. Jpn. J. Med. Imag. Inform. Sci. 20: 148-155, 2003
11) Sato E, Hayasi Y, Germer R, et al.: Irradiation of intense characteristic x-rays from weakly ionized linear molybdenum plasma. Jpn. J. Med. Phys. 23: 123-131, 2003
12) Sato E, Hayasi Y, Germer R, et al.: Quasi-monochromatic flash x-ray generator utilizing weakly

ionized linear copper plasma. Rev. Sci. Instrum. 74: 5236-5240, 2003

13) Xiao Q F and Poturaef S V: Polycapillary-based x-ray optics. Nucl. Instr. Meth. Phys. Res. A 347: 376-383, 1994

14) MacDonald C A, Mail N, Li D, et al.: Monochromatic applications of polycapillary optics. SPIE 5196: 405-411, 2002

15) Sato E, Germer R, Hayasi Y, et al.: Quasi-monochromatic parallel flash radiography achieved with a plane-focus x-ray tube. SPIE 4948: 646-651, 2002

16) Sonoda M, Takano M, Miyahara J, et al.: Computed radiography utilizing scanning laser stimulated luminescence. Radiology 148: 833-838, 1983

17) Sato E, Sato K and Tamakawa Y: Film-less computed radiography system for high-speed imaging. Ann. Rep. Iwate Med. Univ. Sch. Lib. Arts and Sci. 35: 13-23, 2000

Optimal Windows of Statin Use for Immediate Infarct Limitation

5′-Nucleotidase as Another Downstream Molecule of Phosphatidylinositol 3-Kinase

Shoji Sanada, MD, PhD; Hiroshi Asanuma, MD, PhD; Tetsuo Minamino, MD, PhD; Koichi Node, MD, PhD; Seiji Takashima, MD, PhD; Hiroko Okuda, PhD; Yoshiro Shinozaki, MD, PhD; Akiko Ogai, PhD; Masashi Fujita, MD; Akio Hirata, MD; Jiyoong Kim, MD; Yoshihiro Asano, MD, PhD; Hidezo Mori, MD, PhD; Hitonobu Tomoike, MD, PhD; Soichiro Kitamura, MD, PhD; Masatsugu Hori, MD, PhD; Masafumi Kitakaze, MD, PhD

Background—Although statins are reported to have a cardioprotective effect, their immediate direct influence on ischemia-reperfusion injury and the underlying mechanisms remain obscure. We investigated these issues an in vivo canine model.

Methods and Results—Dogs were subjected to coronary occlusion (90 minutes) and reperfusion (6 hours) immediately after injection of pravastatin (0.2, 2, or 10 mg/kg), pitavastatin (0.01, 0.1, or 0.5 mg/kg), or cerivastatin (0.5, 5, or 50 μg/kg). Then myocardial phosphatidylinositol 3-kinase (PI3-K) and 5′-nucleotidase activities were measured, as well as infarct size. After 15 minutes of reperfusion, pravastatin caused dose-dependent activation of Akt and ecto-5′-nucleotidase in the ischemic zone, and the effect was significant at higher doses. Pitavastatin also significantly increased these activities, and its optimal dose was within the clinical range, whereas cerivastatin caused activation at the lowest dose tested. In all cases, both Akt and ecto-5′-nucleotidase showed activation in parallel, and this activation was completely abolished by wortmannin, a PI3-K inhibitor. The magnitude of the infarct-limiting effect paralleled the increase in Akt and ecto-5′-nucleotidase activity and was blunted by administration of wortmannin, α,β-methyleneadenosine-5′-diphosphate, or 8-sulfophenyltheophylline during reperfusion. Both collateral flow and the area at risk were comparable for all groups.

Conclusions—Activation of ecto-5′-nucleotidase after ischemia by PI3-K activation may be crucial for immediate infarct-size limitation by statins. There seems to be an optimal dose for each statin that is independent of its clinical cholesterol-lowering effect. **(*Circulation*. 2004;110:2143-2149.)**

Key Words: statins ■ myocardial infarction ■ adenosine ■ enzymes ■ phosphates

The 3-hydroxy-3-methylglutaryl coenzyme A reductase inhibitors (statins) block the biosynthesis of cholesterol[1] and are widely used clinically to decrease serum cholesterol levels. Recent studies have focused on the pleiotropic effects of either hydrophilic[2-4] or hydrophobic[4,5] statins, which are independent of their cholesterol-lowering effect.[2-4,5] Protection against ischemia-reperfusion injury is one of them, which is particularly evident after 12 hours.[6,7] In addition, some studies showed that statins activate the phosphatidylinositol 3-kinase (PI3-K)/Akt pathway within 1 hour,[8,9] as well as activating endothelial nitric oxide synthase (eNOS),[9,10] to cause immediate infarct limitation.[9]

On the other hand, other studies revealed that statins also acutely activate ecto-5′-nucleotidase,[11] which produces the endogenous cardioprotective substance adenosine,[12] especially in response to certain stresses.[13] Ecto-5′-nucleotidase can act only when localized on the cell membrane,[13] and the density of this enzyme on the membrane regulates its activity.[11,14] Endocytotic turnover of ecto-5′-nucleotidase (5′-nucleotidase localized on the cell surface) is inhibited by PI3-K activation,[14] which subsequently increases total 5′-nucleotidase activity within a period as short as 10 minutes.[14] Therefore, we hypothesized that an increase of ecto-5′-nucleotidase activity might be critical for early cardioprotec-

Received March 26, 2004; revision received May 4, 2004; accepted May 7, 2004

From the Department of Internal Medicine and Therapeutics (S.S., H.A., T.M., S.T., H.O., M.F., A.H., Y.A., M.H.), Osaka University Graduate School of Medicine, Suita; the Department of Cardiovascular and Renal Medicine (K.N.), Saga University Faculty of Medicine, Saga; the Department of Physiological Science (Y.S.), Tokai University School of Medicine, Isehara; and the Cardiovascular Division of Medicine (A.O., J.K., H.M., H.T., S.K., M.K.), National Cardiovascular Center, Suita, Japan

Correspondence to Masafumi Kitakaze, MD, PhD, Director, Cardiovascular Division of Medicine, National Cardiovascular Center, 5-7-1 Fujishirodai, Suita, 565-8565 Japan. E-mail kitakaze@zf6.so-net.ne.jp

Circulation is available at http://www.circulationaha.org

DOI: 10.1161/01.CIR.0000143830.59419.73

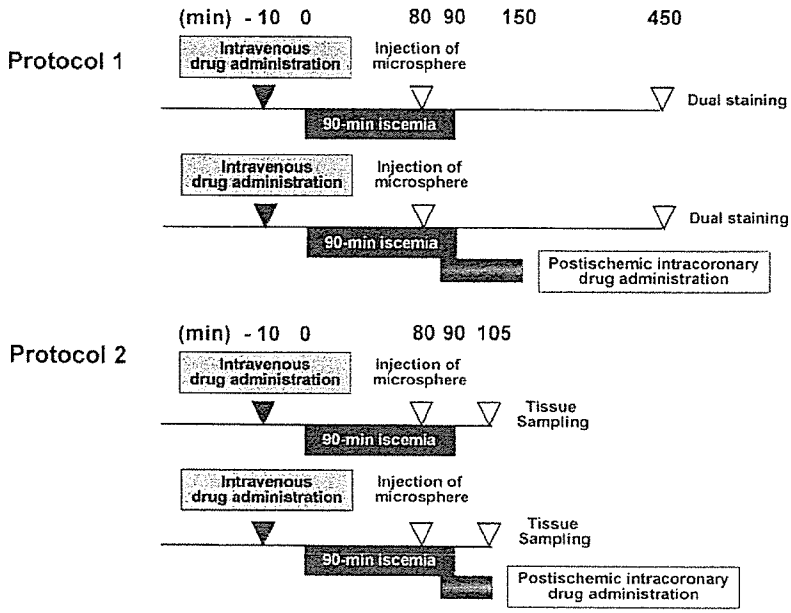

Figure 1. Experimental protocols to measure infarct size (protocol 1; Upper) and kinase activity (protocol 2; Lower).

tion mediated by statins and might be associated with rapid activation of PI3-K.

Here we used a dog model to determine whether 3 statins with different water solubilities (pravastatin, pitavastatin, and cerivastatin) could acutely limit infarct size, as well as whether adenosine and PI3-K were involved in the underlying mechanism.

Methods

All procedures were performed in conformity with the *Guide for the Care and Use of Laboratory Animals* (NIH publication No. 85-23, 1996 revision) and were approved by the Osaka University Committee for Laboratory Animal Use. Pravastatin, pitavastatin, and cerivastatin were obtained from Sankyo, Kowa, and Takeda Pharmaceuticals, respectively. The other drugs were obtained from Sigma.

Instrumentation

Beagle dogs weighing 8 to 13 kg were anesthetized and connected to an extracorporeal bypass tube as described previously.[15,16] In all experiments, the average baseline values of mean aortic blood pressure (ABP), heart rate (HR), and arterial blood Po_2 were 102±2.2 mm Hg, 129±2.5 min^{-1}, and 109±4.1 mm Hg, respectively. Both ABP and HR were measured continuously during the study.

Experimental Protocols

Protocol 1: Measurement of Infarct Size and Myocardial Collateral Blood Flow

After hemodynamic stabilization, we infused pravastatin (0.2, 2, or 10 mg/kg), pitavastatin (0.01, 0.1, or 0.5 mg/kg), cerivastatin (0.5, 5, or 50 μg/kg) or saline intravenously for 10 minutes before 90 minutes of sustained ischemia, which was followed by 6 hours of reperfusion (n=9 to 13 each). Some groups also received intracoronary administration of a selective ecto-5′-nucleotidase inhibitor (α,β-methyleneadenosine-5′-diphosphate [AMP-CP: 80 $\mu g \cdot kg^{-1} \cdot min^{-1}$]; a nonselective adenosine receptor antagonist (8-sulfophenyltheophylline [8-SPT: 50 $\mu g \cdot kg^{-1} \cdot min^{-1}$]); or a selective PI3-K inhibitor (wortmannin [1.5 $\mu g \cdot kg^{-1} \cdot min^{-1}$]) between 5 minutes before and 60 minutes after reperfusion. We measured infarct size and regional myocardial collateral blood flow during 90 minutes of ischemia as described previously.[15]

We have already confirmed in the same model that the doses of AMP-CP,[17] 8-SPT,[17,18] or wortmannin[19] used in this study were appropriate to block ecto-5′-nucleotidase, the adenosine receptors, or PI3-K, respectively. Figure 1 shows the details of this protocol, and the Table lists all of the groups studied.

Protocol 2: Myocardial Enzyme Assays

Another 54 dogs underwent a procedure identical to that of some groups from protocol 1 and were studied for enzyme assays (n=3 or 4 each). In this protocol, not only wortmannin (1.5 $\mu g \cdot kg^{-1} \cdot min^{-1}$) but also LY294002 (60 $\mu g \cdot kg^{-1} \cdot min^{-1}$) was used as another selective PI3-K inhibitor. After 15 minutes of reperfusion, a myocardial tissue sample was obtained from the ischemic border zone to ensure evaluation of viable ischemic myocardium and was used for the measurement of PI3-K and ecto-/endo-5′-nucleotidase activity. The myocardial tissue was rapidly frozen in LN_2 and stored at −80°C. Measurement of PI3-K and 5′-nucleotidase activity was done as reported previously[15,19] with minor modifications.

Criteria for Exclusion

To ensure that all of the animals included in analysis were healthy and were exposed to a similar extent of ischemia, the exclusion criteria reported previously[16] for hemodynamics, excessive collateral flow, and lethal arrhythmia were adopted.

Statistical Analysis

Results were expressed as mean±SEM, and the number of animals or experiments is shown as n. Statistical analysis was performed by ANOVA with a modified Bonferroni post hoc test, and significance was defined at $P<0.05$.

Results

Mortality and Exclusions in Protocol 1

Among 222 dogs used in protocols 1, 56 dogs met the exclusion criteria of ventricular fibrillation or excessive myocardial collateral blood flow (>15 mL · 100 $g^{-1} \cdot min^{-1}$). Therefore, 166 dogs completed these protocols satisfactorily and were included in the data analysis (Table).

Changes in Hemodynamic Parameters, Risk Area, and Collateral Blood Flow in Protocol 1

The changes in ABP and HR were comparable among all groups throughout the protocol (data not shown), and both the

TABLE 1. Mortality, Exclusion, Area at Risk, and Collateral Flow in Each Group in Protocol 1

Groups	Initial No	Excluded: Lethal Arrhythmia: During Ischemia	Excluded: Lethal Arrhythmia: After Reperfusion	Excluded: Excessive Collateral Flow	Final No	Area at Risk, %	Collateral Flow, mL/100 g per minute
Control	13	1	2	1	9	40.1±2.1	8.2±1.0
Prava							
0.2	9	0	1	0	8	38.8±2.0	8.4±1.2
2.0	10	0	0	2	8	39.1±2.2	8.9±1.1
10	10	0	0	2	8	39.6±2.1	8.9±1.4
Pitava							
0.01	9	1	1	0	7	38.7±2.2	8.1±1.3
0.1	11	0	1	2	8	39.3±2.0	9.2±1.5
0.5	10	1	0	2	7	39.9±1.9	8.8±1.5
Ceriva							
0.5	11	0	1	2	8	39.2±1.9	8.5±1.3
5.0	10	1	1	1	7	38.9±2.1	8.7±1.4
50	11	0	1	3	7	39.0 2.0	9.1±1.5
AMP-CP							
+Prava 10	9	0	2	0	7	40.4±2.3	8.6±1.3
+Pitava 0.1	9	0	1	1	7	39.8±2.0	8.4±1.5
+Ceriva 0.5	9	1	1	0	7	40.4±2.3	9.0±1.4
8SPT							
+Prava 10	10	0	1	1	8	38.7±2.2	8.3±1.3
+Pitava 0.1	11	1	2	0	8	39.9±2.1	8.2±1.6
+Ceriva 0.5	11	0	2	1	8	38.4±2.6	8.5±1.5
WTMN							
+Prava 10	10	0	2	1	7	38.6±2.3	9.5±1.5
+Pitava 0.1	10	0	2	0	8	38.9±2.1	9.2±1.6
+Ceriva 0.5	10	0	1	1	8	39.8±2.8	8.8±1.4
AMP-CP	9	0	2	0	7	38.8±2.5	8.5±1.6
8SPT	11	0	3	0	8	39.6±2.5	8.2±1.5
WTMN	9	1	2	0	6	40.5±2.3	8.6±1.6

Data expressed as mean±SEM. Prava indicates pravastatin (mg/kg); Pitava, pitavastatin (mg/kg); Ceriva, cerivastatin (μg/kg); 8SPT, 8-sulfophenyltheophilline; and WTMN, wortmannin.

area at risk and collateral blood flow were also comparable (Table).

Infarct Size

Figure 2 shows infarct size in the groups of protocol 1. Pravastatin (0.2, 2, and 10 mg/kg) dose-dependently reduced the infarct size (29.5±3.5%, 22.5±4.0%, and 18.8±3.4%, respectively) compared with that in the control group (39.8±3.6%), and the difference was significant at 2 mg/kg or more. Pitavastatin (0.01, 0.1, and 0.5 mg/kg) also reduced infarct size (32.9±3.9%, 23.6±3.8%, and 31.4±3.9%, respectively), although the optimal dose was 0.1 mg/kg (the only dose that produced a significant difference). Although cerivastatin (0.5, 5, and 50 μg/kg) caused infarct limitation (26.2±3.2%, 32.1±5.3%, and 37.1±4.4%, respectively), it was significant at the lowest dose only, and the effect was weaker at higher doses. Furthermore, cotreatment with AMP-CP, 8-SPT, or wortmannin between 5 minutes before and 60 minutes after reperfusion abrogated the infarct-limiting effect of pravastatin (39.9±4.0%, 42.6±4.0%, or 38.6±3.6%, respectively), pitavastatin (40.4±3.1%, 39.4±3.6%, or 39.1±3.1%, respectively), and cerivastatin (41.1±3.7%, 42.1±3.9%, or 40.4±4.0%, respectively), although these drugs per se did not affect infarct size (42.7±4.5%, 40.3±3.5%, or 42.7±4.5%, respectively).

5′-Nucleotidase Activity at Reperfusion

Figure 3 shows the activity of ecto-/endo-5′-nucleotidase in protocol 2. Sustained ischemia for 90 minutes and 15 minutes of subsequent reperfusion did not significantly change the activity of ecto-5′-nucleotidase (41.0±5.7 versus 33.2±1.2 nmol · mg protein^{-1} · min^{-1} at baseline). Preischemic treat-

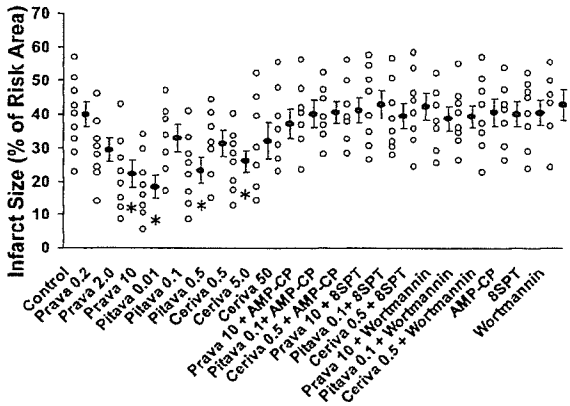

Figure 2. Infarct size in each group in protocol 1. Data are expressed as mean±SEM. *$P<0.05$ vs control. Open circles show infarct size in each individual. Prava indicates pravastatin; Pitava, pitavastatin; and Ceriva; cerivastatin. All other abbreviations are as defined in text.

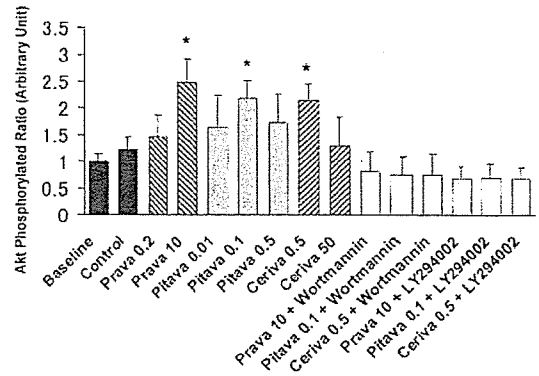

Figure 4. Myocardial PI3-K activity represented by phosphorylated ratio of Akt in each group in protocol 2. Data are expressed as mean±SEM. n=4 each, *$P<0.05$ vs control. Abbreviations are as defined in text and in legend to Figure 2.

ment with pravastatin caused a dose-dependent and acute increase of ecto-5′-nucleotidase activity in the ischemic zone, which became significant at the highest dose (72.6±6.0 nmol · mg protein^{-1} · min^{-1} at 10 mg/kg, $P<0.05$ versus control). Pitavastatin also caused significant activation at its optimal (medium) dose (66.7±6.1 nmol · mg protein^{-1} · min^{-1} at 0.1 mg/kg, $P<0.05$ versus control). Cerivastatin caused activation at the lowest dose (62.5±5.6 nmol · mg protein^{-1} · min^{-1} at 0.5 μg/kg, $P<0.05$ versus control). All of these increases were canceled by the selective PI3-K inhibitors wortmannin (39.5±6.8 nmol · mg protein^{-1} · min^{-1} for pravastatin, 37.0±7.1 nmol · mg protein^{-1} · min^{-1} for pitavastatin, and 38.4±6.5 nmol · mg protein^{-1} · min^{-1} for cerivastatin) or LY294002 (33.5±6.5 nmol · mg protein^{-1} · min^{-1} for pravastatin, 35.0±6.2 nmol · mg protein^{-1} · min^{-1} for pitavastatin, and 37.5±6.7 nmol · mg protein^{-1} · min^{-1} for cerivastatin). The activity of endo-5′-nucleotidase remained unchanged in all cases.

PI3-K Activity at Reperfusion

Figure 4 shows the activity of PI3-K in protocol 2. Sustained ischemia for 90 minutes and subsequent reperfusion for 15 minutes did not change PI3-K activity significantly (123±23% versus 100±14% at baseline). Preischemic treatment with pravastatin caused dose-dependent and acute activation of ecto-5′-nucleotidase in the ischemic zone, which was significant at the highest dose (249±44% at 10 mg/kg, $P<0.05$ versus control). Pitavastatin also caused significant activation at its medium dose (218±34% at 0.1 mg/kg, $P<0.05$ versus control), whereas cerivastatin caused activation at the lowest dose (214±31% at 0.5 μg/kg, $P<0.05$ versus control). We confirmed that all of these increases were also blocked by wortmannin (81±38% for pravastatin,

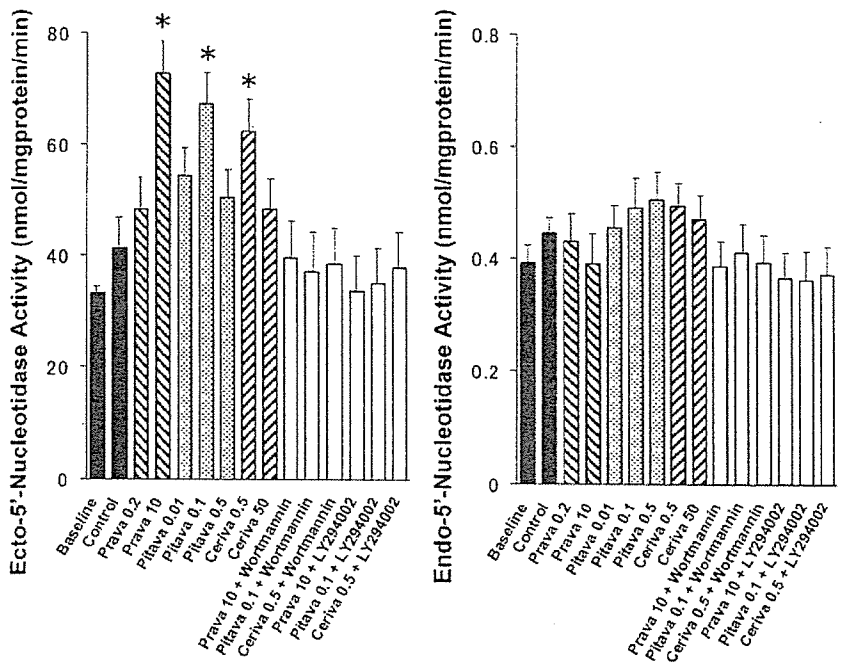

Figure 3. Myocardial ecto-/endo-5′-nucleotidase activity in each group in protocol 2. Data are expressed as mean±SEM. n=4 each, *$P<0.05$ vs control. Abbreviations are as defined in text and in legend to Figure 2.

77±32% for pitavastatin, and 76±39% for cerivastatin) or LY294002 (69±23% for pravastatin, 70±27% for pitavastatin, and 68±21% for cerivastatin).

Discussion

The present study demonstrates that several statins provide immediate infarct limitation of different magnitudes and at different optimal doses. Our results also suggest that activation of ecto-5′-nucleotidase through the activation of PI3-K after ischemia was involved in this cardioprotective mechanism of statins.

Cholesterol-Lowering Effects and Immediate Infarct Limitation of Statins

In this study, we set the doses of statins in line with their clinical cholesterol-lowering properties. In Japan, the standard clinical doses to obtain a 20% to 30% reduction of total plasma cholesterol levels were 10 mg/d for pravastatin, 2 mg/d for pitavastatin, and 0.15 mg/d for cerivastatin. Our preliminary trials in the same dog model revealed that a single intravenous injection of 0.2 mg/kg pravastatin, 0.1 mg/kg pitavastatin, or 5 μg/kg cerivastatin approximated the clinical cholesterol-lowering dose based on the maximal plasma concentration of each statin (data not shown). Because (1) the maximal infarct limitation was achieved by a higher dose of pravastatin than the clinical dose, whereas the dose was similar to the clinical dose for pitavastatin and lower for cerivastatin, and (2) these statins showed early cardioprotection within 2 hours of administration in this model, it is strongly suggested that the magnitude of immediate infarct limitation by each statin is not correlated with its cholesterol-lowering effect.

Existence of Optimal Cardioprotective Doses for Each Statin

In the present report, we have directly shown that pitavastatin has the optimal dose to reduce infarct size. Obviously, there is also an optimal dose for cerivastatin under the lowest dose we tried, because infarct size with far lower doses of cerivastatin near zero will converge with those of control levels. In the case of pravastatin, our additional experiment, within the limitation with regard to the total amount of the drug we could obtain, showed that 100 mg/kg pravastatin administered in the same manner as in protocol 1 exerted similar (but a slightly weaker) magnitude of reducing infarct size (20.9±4.5%, n=5) compared with that achieved with 10 mg/kg of this agent. Although we could not show direct evidence in this case, it would at least not deny the possibility for the existence of an optimal dose of pravastatin. Furthermore, other reports also showed the existence of an optimal dose of atorvastatin for infarct limitation[9] or of simvastatin for PI3-K activation.[8] Taken together, the existence of optimal doses should be ubiquitous among all (or at least all hydrophobic) statins.

Although direct exhibition of the reason for this phenomenon remains unclear in this study, there might be some reasons to regulate the respective optimal windows for each statin, eg, differences in the ability to attenuate inflammatory response[20] or in the potency of direct absorption into cellular membrane to modulate intracellular signaling systems. In addition, our present finding that infarct limitation completely paralleled the activation of PI3-K leads us to hypothesize that the lesser effects by the higher doses of statins should be regulated upstream of PI3-K. One possibility is that all hydrophobic statins can dose-dependently activate apoptosis-related signals,[21] which might also explain the wide range of higher cardioprotective doses for pravastatin specifically. Finally, additional studies will need to be performed to obtain direct evidence.

Cardioprotective Mechanisms

Our observations that (1) activation of PI3-K and ecto-5′-nucleotidase was coincident with a substantial limitation of infarct size, (2) either wortmannin or AMP-CP abolished cardioprotection by all 3 statins, (3) different PI3-K inhibitors at reperfusion actually inhibited PI3-K activity (Figure 4) and subsequently reduced ecto-5′-nucleotidase activity (Figure 3), and (4) our preliminary documentation that PI3-K inhibition by either wortmannin of LY294002 before ischemia did not abolish the infarct limitation by statins in the present study (n=4 or 5, data not shown), together suggest that infarct limitation in this model was linked to the activation of PI3-K during reperfusion, not before ischemia, followed by ecto-5′-nucleotidase activation.

In this study, we did not determine the exact mechanism of how PI3-K activates ecto-5′-nucleotidase. Although we have previously reported that phosphorylation of ecto-5′-nucleotidase might be crucial,[22] other mechanisms may also be involved, such as endocytotic turnover.[17] In addition, although we did not evaluate real-time regional myocardial production of adenosine in each group, treatment with a potent adenosine receptor antagonist (8-SPT) during reperfusion also blunted infarct limitation by statins along with the inhibition of ecto-5′-nucleotidase, further suggesting that cardioprotection against ischemia-reperfusion injury via ecto-5′-nucleotidase activation might be mediated by an increase of adenosine, the main product of ecto-5′-nucleotidase.[11,13,22] However, other implicated mechanism of enhanced activation of the adenosine receptor (eg, increased receptor sensitivity) should be determined by future studies.

Possible Link Between Cardioprotection by Adenosine and NO

Previous studies support our present findings that statins rapidly activate the PI3-K/Akt pathway,[8,9] and we obtained another preliminary finding that the cotreatment with N^{ω}-nitro-L-arginine methyl ester (10 $\mu g \cdot kg^{-1} \cdot min^{-1}$) in the same manner as in protocol 1, which we confirmed did not affect baseline infarct size in the present model,[23] blunted the infarct limitation by pravastatin (36.8±4.1%, n=7), pitavastatin (39.9±3.9%, n=6), and cerivastatin (42.6±4.6%, n=5). Therefore, there is a possibility that ecto-5′-nucleotidase and NO act in series to cause statin-induced cardioprotection.

Although elucidation of a direct effect should be the focus of future studies, there are at least 2 lines of evidence to support the explanation that adenosine and NO synergistically caused infarct limitation in this study. First, NO directly exerts cardioprotection[24]: NO inhibits cell-to-cell adhesion,

such as that between platelets[25] or between neutrophils and endothelial cells,[26,27] by reducing expression of P-selectin,[27] E-selectin, and intercellular adhesion molecule-1,[28] which leads to attenuation of the inflammatory response[22,24,25] or protects against ischemia-reperfusion injury.[25–28] In addition, NO is reported to inhibit caspase-3 activity and to block apoptosis of cardiac myocytes.[29] On the other hand, adenosine also rescues injured myocardium through activating adenosine receptors.[13,30–32] Either administration of adenosine or enhancement of endogenous adenosine release during reperfusion after sustained ischemia limits infarct size.[13,17] We and others have shown that (1) adenosine receptor (A_1 and A_2) activation improves contractile dysfunction after reperfusion,[14] (2) inhibition of norepinephrine release from the presynaptic vesicles and attenuation of calcium influx occur through the A_1 receptor and the coupled inhibitory G protein,[33,34] (3) inhibition of platelet aggregation and leukocyte activation occurs through the A_2 receptor and the coupled stimulatory G protein,[34–36] and (4) activation of extracellular signal–regulated kinase, one of the reperfusion injury survival kinase pathways,[37] takes place during reperfusion through the A_3 receptor.[38] Therefore, either adenosine or NO similarly and potentially protects injured myocardium through multiple pathways.

Second, recent articles have shown that either adenosine[38–40] or NO[41] can reactivate PI3-K downstream. However, increasing the production of both agents is known to negatively regulate further increases of production of these molecules,[42,43] suggesting the requirement of both pathways to confer sufficient cardioprotection in the physiological system. Taking all of these together, it is likely that adenosine and NO synergistically confer the statin-derived immediate cardioprotection shown in this study.

In conclusion, our findings suggest the cellular mechanism by which statins attenuate myocardial injury, which may indicate the possibility of acute protective therapies for ischemia and associated myocardial stresses.

Acknowledgments

This study was supported by grants on the Human Genome, Tissue Engineering and Food Biotechnology (H13-Genome-11) and grants on Comprehensive Research on Aging and Health (H13-21seiki[seikatsu]-23) in Health and Labor Sciences Research from the Ministry of Health, Labor and Welfare; a grant-in-aid for Scientific Research from the Ministry of Education, Culture, Sports, Science and Technology of Japan; and in part by a grant-in-aid for JSPS fellows from the Japan Society for the Promotion of Science and the Japan Heart Foundation.

References

1. Goldstein JL, Brown MS. Regulation of the mevalonate pathway. *Nature*. 1990;343:425–430.
2. Sacks FM, Pfeffer MA, Moye LA, et al. The effect of pravastatin on coronary events after myocardial infarction in patients with average cholesterol levels: Cholesterol and Recurrent Events Trial investigators. *N Engl J Med*. 1996;335:1001–1009.
3. LIPID Study Group. Prevention of cardiovascular events and death with pravastatin in patients with coronary heart disease and a broad range of initial cholesterol levels: the Long-Term Intervention with Pravastatin in Ischaemic Disease (LIPID) Study Group. *N Engl J Med*. 1998;339:1349–1357.
4. 4S Study Group. Randomized trial of cholesterol lowering in 4444 patients with coronary heart disease: the Scandinavian Simvastatin Survival Study (4S). *Lancet* 1994;344:1383–1389.
5. Downs JR, Clearfield M, Weis S, et al. Primary prevention of acute coronary events with lovastatin in men and women with average cholesterol levels: results of AFCAPS/TexCAPS: Air Force/Texas Coronary Atherosclerosis Prevention Study. *JAMA*. 1998;279:1615–1622.
6. Lefer AM, Campbell B, Shin YK, et al. Simvastatin preserves the ischemic-reperfused myocardium in normocholesterolemic rat hearts. *Circulation*. 1999;100:178–184.
7. Ikeda Y, Young LH, Lefer AM. Rosuvastatin, a new HMG-CoA reductase inhibitor, protects ischemic reperfused myocardium in normocholesterolemic rats. *J Cardiovasc Pharmacol*. 2003;41:649–656.
8. Kureishi Y, Luo Z, Shiojima I, et al. The HMG-CoA reductase inhibitor simvastatin activates the protein kinase Akt and promotes angiogenesis in normocholesterolemic animals. *Nat Med*. 2000;6:1004–1010.
9. Bell RM, Yellon DM. Atorvastatin, administered at the onset of reperfusion, and independent of lipid lowering, protects the myocardium by up-regulating a pro-survival pathway. *J Am Coll Cardiol*. 2003;41:508–515.
10. Simoncini T, Genazzani AR, Liao JK. Nongenomic mechanisms of endothelial nitric oxide synthase activation by the selective estrogen receptor modulator raloxifene. *Circulation*. 2002;105:1368–1373.
11. Ledoux S, Laouari D, Essig M, et al. Lovastatin enhances ecto-5′-nucleotidase activity and cell surface expression in endothelial cells: implication of rho-family GTPases. *Circ Res*. 2002;90:420–427.
12. Kitakaze M, Hori M, Morioka T, et al. α′-Adrenoceptor activation mediates the infarct size-limiting effect of ischemic preconditioning through augmentation of 5′-nucleotidase activity. *J Clin Invest*. 1994;93:2197–2205.
13. Kitakaze M, Minamino T, Node K, et al. Adenosine and cardioprotection in the diseased heart. *Jpn Circ J*. 1999;63:231–243.
14. Tuma PL, Finnegan CM, Yi JH, et al. Evidence for apical endocytosis in polarized hepatic cells: phosphoinositide 3-kinase inhibitors lead to the lysosomal accumulation of resident apical plasma membrane proteins. *J Cell Biol*. 1999;145:1089–1102.
15. Kitakaze M, Node K, Minamino T, et al. Role of activation of protein kinase C in the infarct size-limiting effect of ischemic preconditioning through activation of ecto-5′-nucleotidase. *Circulation*. 1996;93:781–791.
16. Sanada S, Kitakaze M, Papst PJ, et al. Role of phasic dynamism of P38 mitogen-activated protein kinase activation in the ischemic preconditioning on the canine heart. *Circ Res*. 2001;88:175–180.
17. Kitakaze M, Minamino T, Funaya H, et al. Vesnarinone limits infarct size via adenosine-dependent mechanisms in the canine heart. *Circulation*. 1997;95:2108–2114.
18. Node K, Kitakaze M, Minamino T, et al. Activation of ecto-5′-nucleotidase by protein kinase C and its role in ischaemic tolerance in the canine heart. *Br J Pharmacol*. 1997;120:273–281.
19. Ogita H, Node K, Asanuma H, et al. Raloxifene improves coronary perfusion, cardiac contractility and myocardial metabolism in the ischemic heart: role of phosphatidylinositol 3-kinase/Akt pathway. *J Cardiovasc Pharmacol*. 2004;43:821–829.
20. Hilgendorff A, Muth H, Parviz B, et al. Statins differ in their ability to block NF-κB activation in human blood monocytes. *Int J Clin Pharmacol Ther*. 2003;41:397–401.
21. Kaneta S, Satoh K, Kano S, et al. All hydrophobic HMG-CoA reductase inhibitors induce apoptotic death in rat pulmonary vein endothelial cells. *Atherosclerosis*. 2003;170:237–243.
22. Kitakaze M, Minamino T, Node K, et al. Activation of ecto-5′-nucleotidase and cardioprotection of ischemic preconditioning. *Basic Res Cardiol*. 1996;91:23–26.
23. Asanuma H, Kitakaze M, Funaya H, et al. Nifedipine limits infarct size via NO-dependent mechanisms in dogs. *Basic Res Cardiol*. 2001;96:497–505.
24. Lefer AM, Lefer DJ. Nitric oxide, II: nitric oxide protects in intestinal inflammation. *Am J Physiol*. 1999;276:G572–G575.
25. Massberg S, Sausbier M, Klatt P, et al. Increased adhesion and aggregation of platelets lacking cyclic guanosine 3′,5′-monophosphate kinase I. *J Exp Med*. 1999;189:1255–1264.
26. Agullo L, Garcia-Dorado D, Inserte J, et al. L-Arginine limits myocardial cell death secondary to hypoxia-reoxygenation by a cGMP-dependent mechanism. *Am J Physiol*. 1999;276:H1574–H1580.

27. Jordan JE, Zhao ZQ, Vinten-Johansen J. The role of neutrophils in myocardial ischemia-reperfusion injury. *Cardiovasc Res*. 1999;43: 860–878.
28. Buras JA, Stahl GL, Svoboda KK, et al. Hyperbaric oxygen down-regulates ICAM-1 expression induced by hypoxia and hypoglycemia: the role of NOS. *Am J Physiol Cell Physiol*. 2000;278:C292–C302.
29. Weiland U, Haendeler J, Ihling C, et al. Inhibition of endogenous nitric oxide synthase potentiates ischemia-reperfusion–induced myocardial apoptosis via a caspase-3 dependent pathway. *Cardiovasc Res*. 2000;45: 671–678.
30. Dorheim TA, Hoffman A, Van Wylen DG, et al. Enhanced interstitial fluid adenosine attenuates myocardial stunning. *Surgery*. 1991;110: 136–145.
31. Babbitt DG, Virmani R, Vildibill HD Jr, et al. Intracoronary adenosine administration during reperfusion following 3 hours of ischemia: effects on infarct size, ventricular function, and regional myocardial blood flow. *Am Heart J*. 1990;120:808–818.
32. Norton ED, Jackson EK, Virmani R, et al. Effect of intravenous adenosine on myocardial reperfusion injury in a model with low myocardial collateral blood flow. *Am Heart J*. 1991;122:1283–1291.
33. Richardt G, Waas W, Kranzhofer R, et al. Adenosine inhibits exocytotic release of endogenous noradrenaline in rat heart: a protective mechanism in early myocardial ischemia. *Circ Res*. 1987;61:117–123.
34. Sato H, Hori M, Kitakaze M, et al. Endogenous adenosine blunts β-adrenoceptor–mediated inotropic response in hypoperfused canine myocardium. *Circulation*. 1992;85:1594–1603.
35. Cronstein BN, Levin RI, Belanoff J, et al. Adenosine: an endogenous inhibitor of neutrophil-mediated injury to endothelial cells. *J Clin Invest*. 1986;78:760–770.
36. Kitakaze M, Hori M, Sato H, et al. Endogenous adenosine inhibits platelet aggregation during myocardial ischemia. *Circ Res*. 1991;69:1402–1408.
37. Hausenloy DJ, Yellon DM. New directions for protecting the heart against ischaemia-reperfusion injury: targeting the reperfusion injury salvage kinase (RISK)-pathway. *Cardiovasc Res*. 2004;61:448–460.
38. Trincavelli ML, Tuscano D, Marroni M, et al. Involvement of mitogen protein kinase cascade in agonist-mediated human A_3 adenosine receptor regulation. *Biochim Biophys Acta*. 2002;1591:55–62.
39. Yang XM, Krieg T, Cui L, et al. NECA and bradykinin at reperfusion reduce infarction in rabbit hearts by signaling through PI3K, ERK, and NO. *J Mol Cell Cardiol*. 2004;36:411–421.
40. Boucher M, Pesant S, Falcao S, et al. Post-ischemic cardioprotection by A2A adenosine receptors: dependent of phosphatidylinositol 3-kinase pathway. *J Cardiovasc Pharmacol*. 2004;43:416–422.
41. Kawasaki K, Smith RS Jr, Hsieh CM, et al. Activation of the phosphatidylinositol 3-kinase/protein kinase Akt pathway mediates nitric oxide–induced endothelial cell migration and angiogenesis. *Mol Cell Biol*. 2003;23:5726–5737.
42. Richardt G, Waas W, Kranzhofer R, et al. Interaction between the release of adenosine and noradrenaline during sympathetic stimulation: a feed-back mechanism in rat heart. *J Mol Cell Cardiol*. 1989;21:269–277.
43. Buga GM, Griscavage JM, Rogers NE, et al. Negative feedback regulation of endothelial cell function by nitric oxide. *Circ Res*. 1993;73: 808–812.

Weakly ionized cerium plasma radiography

Eiichi Sato[a], Yasuomi Hayasi[a], Rudolf Germer[b], Yoshitake Koorikawa[a], Kazunori Murakami[a], Etsuro Tanaka[c], Hidezo Mori[d], Toshiaki Kawai[e], Toshio Ichimaru[f], Fumiko Obata[g], Kiyomi Takahashi[g], Sigehiro Sato[g], Kazuyoshi Takayama[h] and Hideaki Ido[i]

[a]Department of Physics, Iwate Medical University, 3-16-1 Honchodori, Morioka 020-0015, Japan
[b]ITP, FHTW FB1 and TU-Berlin, Blankenhainer Str. 9, D 12249 Berlin, Germany
[c]Department of Nutritional Science, Faculty of Applied Bio-science, Tokyo University of Agriculture, 1-1-1 Sakuragaoka, Setagaya-ku 156-8502, Japan
[d]Department of Cardiac Physiology, National Cardiovascular Center Research Institute, 5-7-1 Fujishiro-dai, Suita, Osaka 565-8565, Japan
[e]Electron Tube Division #2, Hamamatsu Photonics Inc., 314-5 Shimokanzo, Toyooka Village, Iwata-gun 438-0193, Japan
[f]Department of Radiological Technology, School of Health Sciences, Hirosaki University, 66-1 Honcho, Hirosaki 036-8564, Japan
[g]Department of Microbiology, School of Medicine, Iwate Medical University, 19-1 Uchimaru, Morioka 020-8505, Japan
[h]Shock Wave Research Center, Institute of Fluid Science, Tohoku University, 2-1-1 Katahira, Aoba-ku, Sendai 980-8577, Japan
[i]Department of Applied Physics, Faculty of Engineering, Tohoku Gakuin University, 1-13-1 Chuo, Tagajo 985-8537, Japan

ABSTRACT

In the plasma flash x-ray generator, high-voltage main condenser of about 200 nF is charged up to 55 kV by a power supply, and electric charges in the condenser are discharged to an x-ray tube after triggering the cathode electrode. The flash x-rays are then produced. The x-ray tube is of a demountable triode that is connected to a turbo molecular pump with a pressure of approximately 1 mPa. As electron flows from the cathode electrode are roughly converged to a rod cerium target of 3.0 mm in diameter by electric field in the x-ray tube, the weakly ionized linear plasma, which consists of cerium ions and electrons, forms by target evaporating. At a charging voltage of 55 kV, the maximum tube voltage was almost equal to the charging voltage of the main condenser, and the peak current was about 20 kA. When the charging voltage was increased, weakly ionized cerium plasma formed, and the K-series characteristic x-ray intensities increased. The x-ray pulse widths were about 500 ns, and the time-integrated x-ray intensity had a value of about 40 μC/kg at 1.0 m from x-ray source with a charging voltage of 55 kV. In the angiography, we employed a film-less computed radiography (CR) system and iodine-based microspheres. Because K-series characteristic x-rays are absorbed easily by the microspheres, high-contrast angiography has been performed.

Key words: Plasma x-ray, cerium target, weakly ionized cerium plasma, characteristic x-ray, high contrast angiography

Ultrahigh- and High-Speed Photography, Photonics, and Videography, edited by Donald R. Snyder, Proc. of SPIE Vol. 5210 (SPIE, Bellingham, WA, 2004) · 0277-786X/04/$15 · doi: 10.1117/12.506563

1. INTRODUCTION

Flash x-rays are useful in order to perform high-speed radiography, and various generators have been developed to correspond to specific radiographic objectives.[1-6] In the cases of multiple-shot and cine radiographies, we have developed several different repetitive-flash[7-11] and stroboscopic x-ray generators.[12-18] Although most flash x-ray generators have cold-cathode tubes, the stroboscopic generators utilize hot-cathode tubes.

In conjunction with single crystals, synchrotrons generate monochromatic x-rays. These rays play important roles in parallel radiography and have been employed to perform high-contrast micro-angiography[19] and x-ray phase imaging.[20,21] However, it is difficult to obtain sufficient machine times for various research projects including medical applications.

As for angiography using iodine-based contrast mediums, K-series characteristic x-rays of cerium are extremely useful, since the rays are absorbed easily by iodine. In particular, since quite intense and sharp characteristic x-rays have been produced from weakly ionized linear plasmas[22-25] of nickel, copper and molybdenum, the development of a cerium-target x-ray tube for angiography is highly desirable.

In this research, we developed a single flash x-ray generator with a cerium-target plasma tube and performed a tentative study on weakly ionized cerium plasma angiography.

2. GENERATOR

2.1 High-voltage circuit

Figure 1 shows block diagram of a high-intensity plasma flash x-ray generator. This generator consists of the following essential components: a high-voltage power supply, a high-voltage condenser with a capacity of about 200 nF, a turbo-molecular pump, a krytron pulse generator as a trigger device, and a flash x-ray tube. In this generator, a low-impedance transmission line is employed in order to increase maximum tube current. The high-voltage main condenser is charged up to 55 kV by the power supply, and electric charges in the condenser are discharged to the tube after triggering the cathode electrode by the trigger device. The plasma flash x-rays are then produced.

2.2 X-ray tube

The x-ray tube is a demountable cold-cathode triode that is connected to the turbo molecular pump with a pressure of approximately 1 mPa (Fig. 2). This tube consists of the following major parts: a pipe-shaped carbon cathode with a bore diameter of 10.0 mm, a trigger electrode made from a copper wire, a stainless-steel vacuum chamber, a nylon insulator, a polyethylene terephthalate (Mylar) x-ray window of 0.25 mm, and a rod-shaped cerium target of 3.0 mm in diameter. The target tip is embedded in the carbon rod in order to absorb the characteristic x-rays of carbon by the window. The distance between the target and cathode electrodes is approximately 20 mm, and the trigger electrode is set in the cathode electrode. As electron beams from the cathode electrode are roughly converged to the target by electric field in the tube, the weakly ionized plasma, which consists of cerium ions and electrons, forms around the target by evaporating.

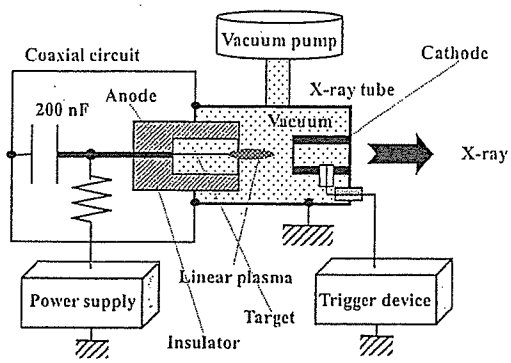

Figure 1: Block diagram of high-intensity plasma flash x-ray generator.

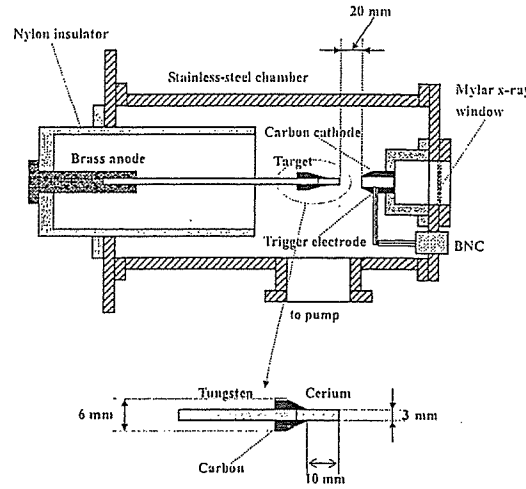

Figure 2: Schematic drawing of flash x-ray tube with a rod target.

3. CHARACTERISTICS

3.1 Tube voltage and current

Tube voltage and current were measured by a high-voltage divider with an input impedance of 1 GΩ and a current transformer, respectively. Figure 3 shows time relation between the tube voltage and current. At the indicated charging voltages, they roughly displayed damped oscillations. When the charging voltage was increased, both the maximum tube voltage and current increased. At a charging voltage of 55 kV, the maximum tube voltage was almost equal to the charging voltage of the main condenser, and the maximum tube current was about 20 kA.

3.2 X-ray output

X-ray output pulse was detected using a combination of a plastic scintillator and a photomultiplier. The x-ray pulse height substantially increased with corresponding increases in the charging voltage (Fig. 4). The x-ray pulse widths were about 500 ns, and the time-integrated x-ray intensity measured by a thermoluminescence dosimeter (Kyokko TLD Reader 1500 utilizing MSO-S elements without energy compensation) had a value of about 40 μC/kg at 1.0 m from the x-ray source with a charging voltage of 55 kV.

3.3 X-ray source

In order to measure images of the plasma x-ray source, we employed a pinhole camera with a hole diameter of 100 μm (Fig. 5). When the charging voltage was increased, the plasma x-ray source grew, and both spot dimension and intensity increased. In contrast, both the dimension and intensity decreased according to insertion of the monochromatic filter.

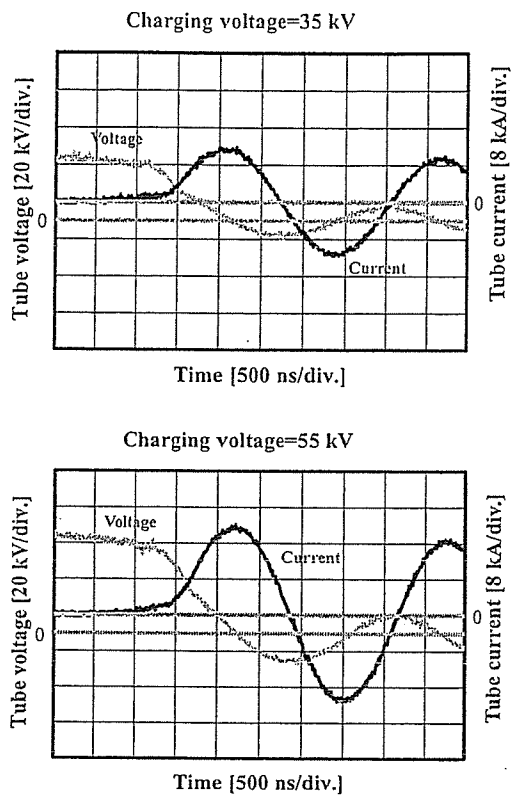

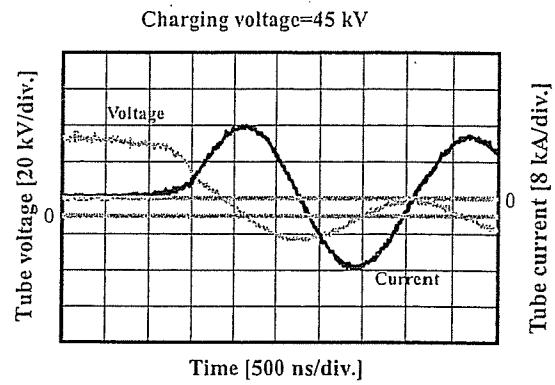

Figure 3: Tube voltages and currents at the indicated charging voltages.

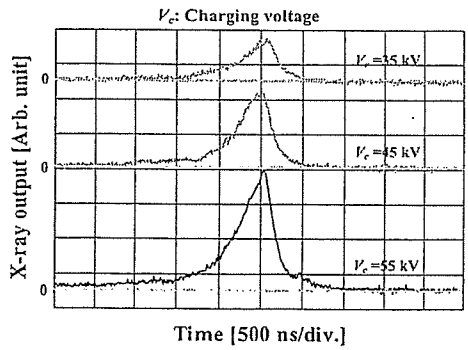

Figure 4: X-ray outputs at the indicated conditions.

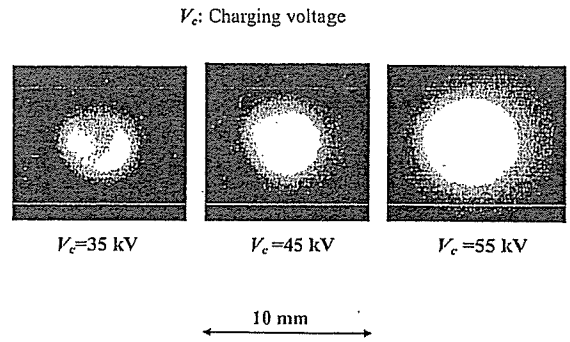

Figure 5: Images of plasma x-ray source.

3.4 X-ray spectra

X-ray spectra from the plasma source were measured by a transmission-type spectrometer with a lithium fluoride curved crystal of 0.5 mm in thickness (Fig. 6). The spectra were taken by a computed radiography (CR) system[26] (Konica Regius 150) having a wide dynamic range, and relative x-ray intensity was calculated from Dicom digital data. Figure 7 shows measured spectra from the cerium target. In this experiment, although we observed both the bremsstrahlung and characteristic x-rays, we could not observe characteristic x-rays with a charging voltage of 35 kV

because the critical excitation energy is 40.3 keV. Both the intensities increased substantially with increases in the charging voltage.

3.5 X-ray divergence by slits

In order to ascertain difference of characteristics between x-rays from a conventional tube and these from the plasma tube, we employed two lead slits in order to measure the divergence of the x-rays (Fig. 8). As compared with x-rays from a conventional tube having a tungsten target, the characteristic x-rays from the plasma were diffused greatly after passing through two slits (Fig. 9).

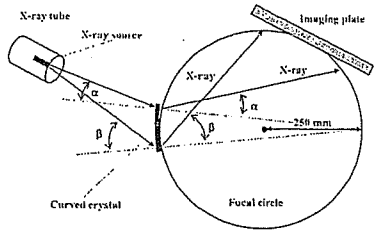

Figure 6: Transmission-type spectrometer with a lithium fluoride curved crystal and an imaging plate.

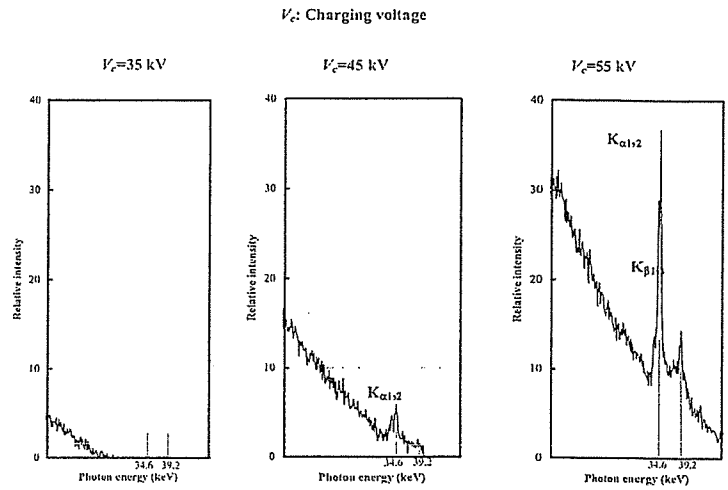

Figure 7: X-ray spectra from weakly ionized cerium plasma.

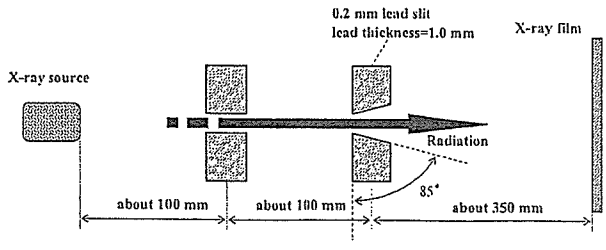

Figure 8: Experimental setup for measuring x-ray divergence using two lead slits.

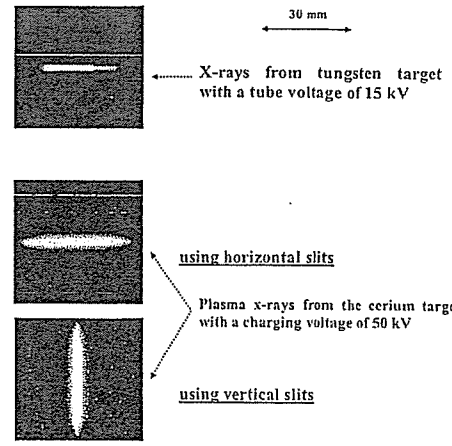

Figure 9: X-ray divergence by two lead slits.

4. ANGIOGRAPHY

The plasma angiography was performed by the CR system without using a monochromatic filter, and the distance between the x-ray source and the imaging plate was 1.2 m.

Firstly, rough measurements of image resolution were made using wires. Figure 10 shows radiograms of 50 μm-diameter tungsten wires coiled around a pipe and a rod made of polymethyl methacrylate (PMMA) with a charging voltage of 55 kV. Although the image contrast increased using the pipe, 50 μm-diameter wires could be observed.

The image of water falling into a polypropylene beaker from a glass test tube is shown in Fig. 11. This image was taken with a charging voltage of 55 kV, with the slight addition of an iodine-based contrast medium. Because the x-ray duration was about 1 μs, the stop-motion image of water could be obtained.

Angiograms of rabbit hearts are shown in Fig. 12. These two images were obtained using iodine and cerium microspheres of 20 μm, respectively, with a charging voltage of 55 kV. In case where the cerium spheres were employed, the coronary arteries were barely visible. Figure 13 shows an angiogram of the external ear of a rabbit using iodine spheres with a charging voltage of 55 kV, and fine blood vessels of about 50 μm are clearly visible. In angiography of a larger heart extracted from a dog, using iodine spheres, a PMMA plate was set in front of heart facing x-ray source, and image contrast of coronary arteries increased with increases in the plate thickness (Fig. 14).

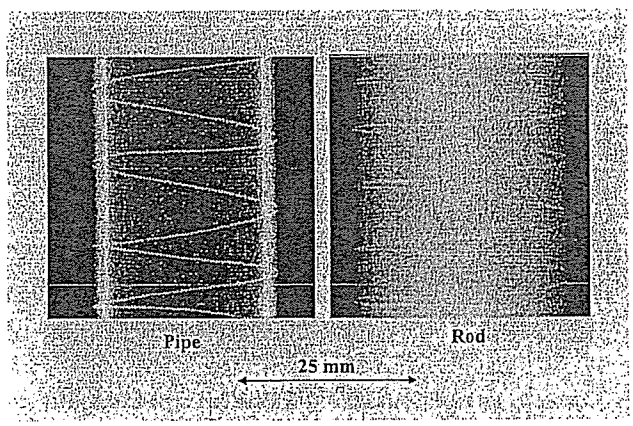

Figure 10: Radiograms of tungsten wires of 50 μm in diameter coiled around pie and a rod made of PMMA.

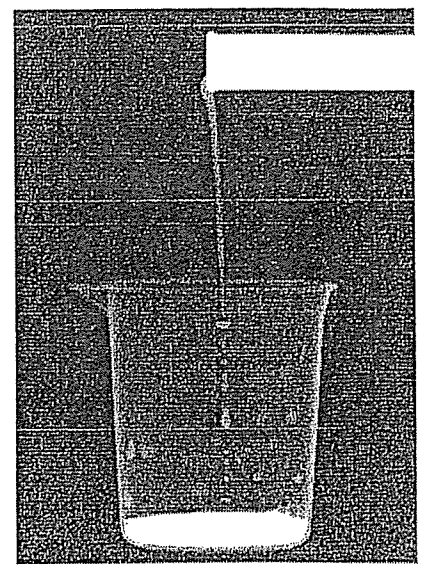

Figure 11: Radiogram of water falling into a polypropylene beaker from a glass test tube.

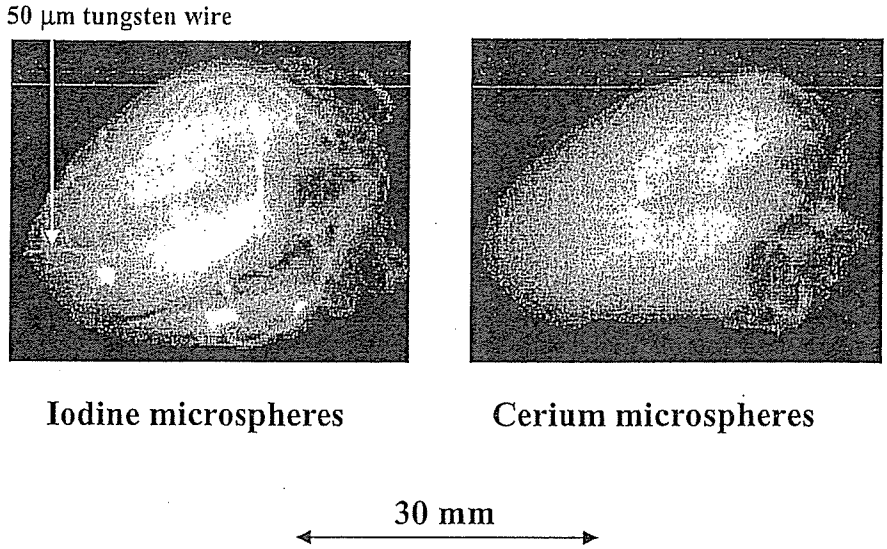

Figure 12: Angiograms of rabbit hearts using iodine and cerium microspheres.

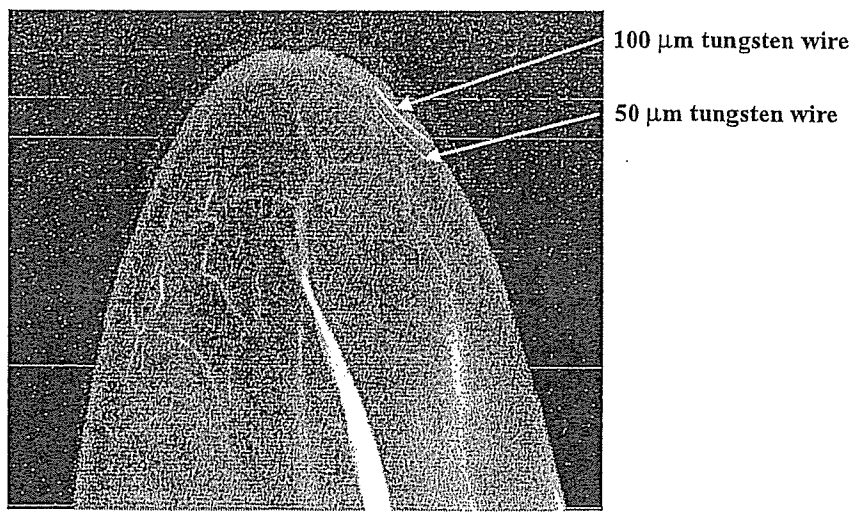

Figure 13: Angiograms of the external ear of a rabbit.

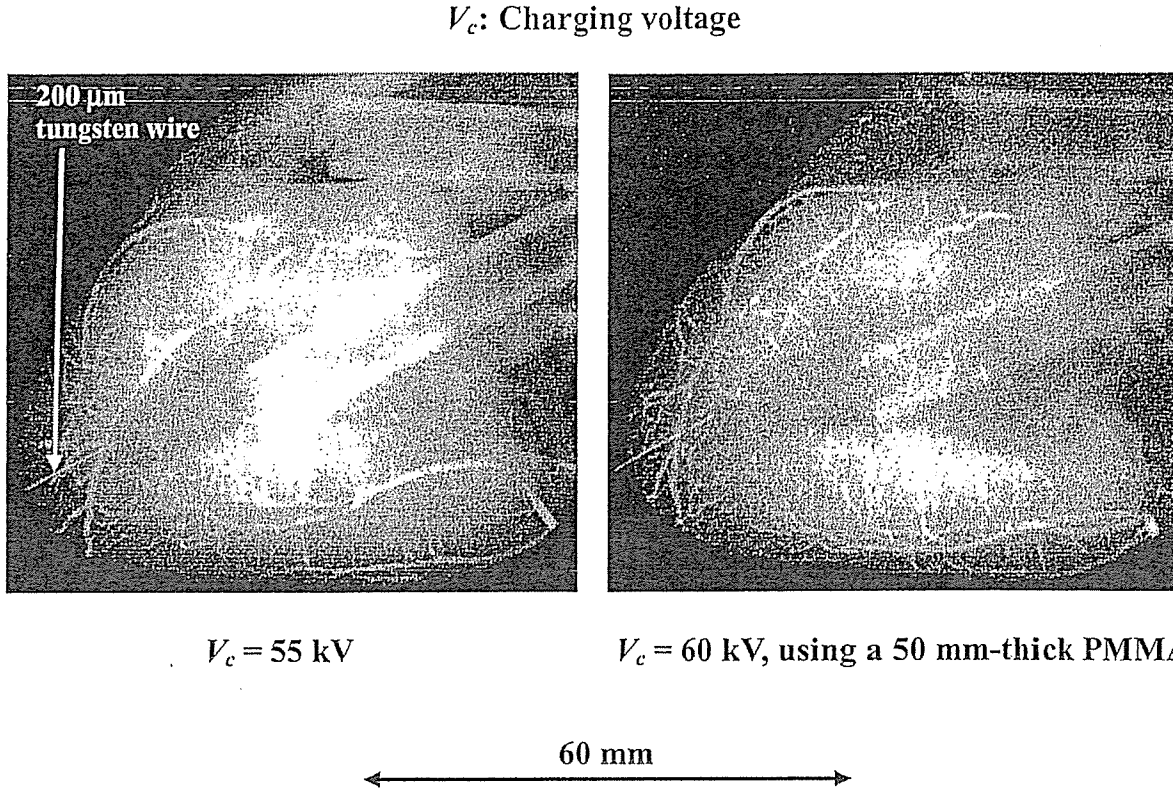

Figure 14: Angiograms of an extracted heart of a dog.

5. DISCUSSION

Cerium is a rare earth element and has a high reactivity. However, the average photon energy of K_α lines is 34.566 keV, and iodine spheres with a K-absorption edge of 33.155 keV absorb the lines easily (Fig. 15). Next, since the spheres easily transmit bremsstrahlung x-rays with energies of lower than the edge, it is important that the rays be absorbed as much as possible before angiography in order to increase the image contrast.

In an earlier experiment using a copper target,[23] bremsstrahlung x-rays were hardly observed at all, and we confirmed the irradiation of quite sharp and intense K-series characteristic x-rays such as lasers. In the present work, although we confirmed intense characteristic x-rays with a higher charging voltage, bremsstrahlung x-rays were detected, since the bremsstrahlung intensity is proportional to the atomic number of the target element. Therefore, the condenser charging voltage should be raised as high as possible to increase the characteristic x-ray intensity. In order to decrease emission of bremsstrahlung x-rays from the carbon target holder, the target length should also be set as long as possible.

In this research, we obtained sufficient x-ray intensity per pulse for CR radiography, and the generator produced high-dose-rate plasma x-rays of approximately 80 C/kg·s at 1.0 m with a charging voltage of 55 kV. In addition, because the x-ray intensity increases with increases in the electrostatic energy in the main discharge condenser, the flash x-rays from weakly ionized linear cerium plasma can be employed to perform high-speed angiography for cardiovascular disease.

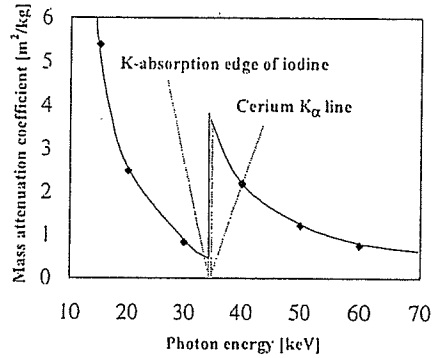

Figure 15: Relation between the mass attenuation coefficient of iodine and the average photon energy of cerium K_α lines.

ACKOWLEDGEMENTS

This work was supported by Grants-in-Aid for Scientific Research (12670902, 13470154, and 13877114) and Advanced Medical Scientific Research from MECSST, Grants from Keiryo Research Foundation, JST (Test of Fostering Potential), NEDO, and MHLW (HLSRG, RAMT-nano-001, RHGTEFB-genome-005, and RGCD13C-1).

REFERENCES

1. A. Mattsson, "Some characteristics of a 600 kV flash x-ray tube," *Physica Scripta*, **5**, pp. 99-102, 1972.

2. R. Germer, "X-ray flash techniques," *J. Phys. E: Sci. Instrum.*, **12**, pp. 336-350, 1979.

3. E. Sato, H. Isobe and F. Hoshino, "High intensity flash x-ray apparatus for biomedical radiography," *Rev. Sci. Instrum.*, **57**, pp. 1399-1408, 1986.

4. E. Sato, M. Sagae, K. Takahashi, T. Oizumi, H. Ojima, K. Takayama, Y. Tamakawa, T. Yanagisawa, A. Fujiwara and K. Mitoya, "High-speed soft x-ray generators in biomedicine," *SPIE*, **2513**, pp. 649-667, 1994.

5. E. Sato, M. Sagae, K. Takahashi, A. Shikoda, T. Oizumi, H. Ojima, K. Takayama, Y. Tamakawa, T. Yanagisawa, A. Fujiwara and K. Mitoya, "Dual energy flash x-ray generator," *SPIE*, **2513**, pp. 723-735, 1994.

6. E. Sato, M. Sagae, A. Shikoda, K. Takahashi, T. Oizumi, M. Yamamoto, A. Takabe, K. Sakamaki, Y. Hayasi, H. Ojima, K. Takayama and Y. Tamakawa, "High-speed soft x-ray techniques," *SPIE*, **2869**, pp. 937-955, 1996.

7. E. Sato, S. Kimura, S. Kawasaki, H. Isobe, K. Takahashi, Y. Tamakawa and T. Yanagisawa, "Repetitive flash x-ray generator utilizing a simple diode with a new type of energy-selective function," *Rev. Sci. Instrum.*, **61**, pp. 2343-2348, 1990.

8. S. Kimura, E. Sato, M. Sagae, A. Shikoda, T. Oizumi, K. Takahashi, Y. Tamakawa and T. Yanagisawa, "Disk-cathode flash x-ray tube driven by a repetitive two-stage Marx pulser," *Med. & Biol. Eng. & Comput.*, **31**, pp. S37-S43, 1993.

9. A. Shikoda, E. Sato, M. Sagae, T. Oizumi, Y. Tamakawa and T. Yanagisawa, "Repetitive flash x-ray generator having a high-durability diode driven by a two-cable-type line pulser," *Rev. Sci. Instrum.*, **65**, pp. 850-856, 1994.

10. E. Sato, K. Takahashi, M. Sagae, S. Kimura, T. Oizumi, Y. Hayasi, Y. Tamakawa and T. Yanagisawa, "Sub-kilohertz flash x-ray generator utilizing a glass-enclosed cold-cathode triode," *Med. & Biol. Eng. & Comput.*,

32, pp. 289-294, 1994.

11. K. Takahashi, E. Sato, M. Sagae, T. Oizumi, Y. Tamakawa and T. Yanagisawa, "Fundamental study on a long-duration flash x-ray generator with a surface-discharge triode," *Jpn. J. Appl. Phys.*, **33**, pp. 4146-4151, 1994.

12. E. Sato, A. Shikoda, S. Kimura, M. Sagae, H. Isobe, Y. Tamakawa and T. Yanagisawa, "Kilohertz-range flash x-ray generator utilizing a triode in conjunction with an extremely hot cathode," *Rev. Sci. Instrum.*, **62**, pp. 2115-2120, 1991.

13. E. Sato, M. Sagae, K. Takahashi, A. Shikoda, T. Oizumi, Y. Hayasi, Y. Tamakawa and T. Yanagisawa, "10 kHz microsecond pulsed x-ray generator utilizing a hot-cathode triode with variable durations for biomedical radiography," *Med. & Biol. Eng. & Comput.*, **32**, pp. 295-301, 1994.

14. E. Sato, T. Ichimaru, T. Usuki, K. Sato, H. Ojima, K. Takayama, H. Ido, K. Sakamaki and Y. Tamakawa, "Condenser-discharge stroboscopic x-ray generator SX-C98," *SPIE*, **3516**, pp. 618-625, 1998.

15. E. Sato. T. Ichimaru, H. Ojima, K. Takayama, H. Ido and Y. Tamakawa, "Characteristics of the kilohertz-range harder stroboscopic x-ray generator and applications," *SPIE*, **3771**, pp. 12-21, 1999.

16. E. Sato, T. Ichimaru, H. Obara, M. Zuguchi, H. Mori, E. Tanaka, T. Usuki, K. Sato, H. Ojima, K. Takayama, K. Sakamaki and Y. Tamakawa, "Condenser-discharge stroboscopic x-ray generator for medical radiography," *SPIE*, **4183**, pp. 383-393, 2000.

17. E. Sato, H. Ojima, K. Takayama, M. Matsumasa, H. Obara, M. Zuguchi, T. Usuki, K. Sato, K. Sakamaki and Y. Tamakawa, "Observation of cavitation bubble cloud using a stroboscopic x-ray generator," *SPIE*, **4183**, pp. 394-404, 2000.

18. E. Sato, Y. Hayasi and Y. Tamakawa, "Recent stroboscopic x-ray generators and their applications to high-speed radiography," *Ann. Rep. Iwate Med. Univ. Lib. Arts and Sci.*, **35**, pp. 1-11, 2000.

19. H. Mori, K. Hyodo, E. Tanaka, M.U. Mohammed, A. Yamakawa, Y. Shinozaki, H. Nakazawa, Y. Tanaka, T. Sekka, Y. Iwata, S. Honda, K. Umetani, H. Ueki, T. Yokoyama, K. Tanioka, M. Kubota, H. Hosaka, N. Ishizawa and M. Ando, "Small-vessel radiography in situ with monochromatic synchrotoron radiation," *Radiology*, **201**, pp. 173-177, 1996.

20. T.J. Davis, D. Gao, T.E. Gureyev, A.W. Stevenson and S.W. Wilkims, "Phase-contrast imagimg of weakly absorbing materials using hard x-rays," *Nature*, **373**, pp. 595-597, 1995.

21. A. Momose, T. Takeda, Y. Itai and K. Hirano, "Phase-contrast x-ray computed tomography for observing biological soft tissues," *Nature Medicine*, **2(4)**, pp. 473-475, 1996.

22. E. Sato, Y. Suzuki, Y. Hayashi, E. Tanaka, H. Mori, T. Kawai, K. Takayama, H. Ido and Y. Tamakawa, "High-intensity quasi-monochromatic x-ray irradiation from the linear plasma target," *SPIE*, **4505**, pp. 154-164, 2001.

23. E. Sato, Y. Hayashi, E. Tanaka, H. Mori, T. Kawai, H. Obara, T. Ichimaru, K. Takayama, H. Ido, T. Usuki, K. Sato and Y. Tamakawa, "Polycapillary radiography using a quasi-x-ray laser generator," *SPIE*, **4508**, pp. 176-187, 2001.

24. E. Sato, Y. Hayasi, E. Tanaka, H. Mori, T. Kawai, T. Usuki, K. Sato, H. Obara, T. Ichimaru, K. Takayama, H. Ido and Y. Tamakawa, "Quasi-monochromatic radiography using a high-intensity quasi-x-ray laser generator," *SPIE*, **4682**, pp. 538-548 2002.

25. E. Sato, Y. Hayasi, R. Germer, E. Tanaka, H. Mori, T. Kawai, H. Obara, T. Ichimaru, K. Takayama and H. Ido, "Intense characteristic x-ray irradiation from weakly ionized linear plasma and applications," *Jpn. J. Med. Imag. Inform. Sci.*, **20**, pp. 148-155. 2003.

26. E. Sato , K. Sato and Y. Tamakawa, "Film-less computed radiography system for high-speed Imaging," *Ann. Rep. Iwate Med. Univ. Sch. Lib. Arts and Sci.*, **35**, pp. 13-23, 2000.

Weakly ionized plasma flash x-ray generator and its distinctive characteristics

Eiichi Sato[a], Yasuomi Hayasi[a], Rudolf Germer[b], Kazunori Murakami[a], Yoshitake Koorikawa[a], Etsuro Tanaka[c], Hidezo Mori[d], Toshiaki Kawai[e], Toshio Ichimaru[f], Fumiko Obata[g], Kiyomi Takahashi[g], Sigehiro Sato[g], Kazuyoshi Takayama[h] and Hideaki Ido[i]

[a]Department of Physics, Iwate Medical University, 3-16-1 Honchodori, Morioka 020-0015, Japan
[b] ITP, FHTW FB1 and TU-Berlin, Blankenhainer Str. 9, D 12249 Berlin, Germany
[c] Department of Nutritional Science, Faculty of Applied Bio-science, Tokyo University of Agriculture, 1-1-1 Sakuragaoka, Setagaya-ku 156-8502, Japan
[d] Department of Cardiac Physiology, National Cardiovascular Center Research Institute, 5-7-1 Fujishiro-dai, Suita, Osaka 565-8565, Japan
[e] Electron Tube Division #2, Hamamatsu Photonics Inc., 314-5 Shimokanzo, Toyooka Village, Iwata-gun 438-0193, Japan
[f] Department of Radiological Technology, School of Health Sciences, Hirosaki University, 66-1 Honcho, Hirosaki 036-8564, Japan
[g] Department of Microbiology, School of Medicine, Iwate Medical University, 19-1 Uchimaru, Morioka 020-8505, Japan
[h] Shock Wave Research Center, Institute of Fluid Science, Tohoku University, 2-1-1 Katahira, Aoba-ku, Sendai 980-8577, Japan
[i] Department of Applied Physics, Faculty of Engineering, Tohoku Gakuin University, 1-13-1 Chuo, Tagajo 985-8537, Japan

ABSTRACT

In the plasma flash x-ray generator, a high-voltage main condenser of approximately 200 nF is charged up to 50 kV by a power supply, and electric charges in the condenser are discharged to an x-ray tube after triggering the cathode electrode. The flash x-rays are then produced. The x-ray tube is a demountable triode that is connected to a turbo molecular pump with a pressure of approximately 1 mPa. As electron flows from the cathode electrode are roughly converged to a rod copper target of 3.0 mm in diameter by the electric field in the x-ray tube, weakly ionized linear plasma, which consists of copper ions and electrons, forms by target evaporation. At a charging voltage of 50 kV, the maximum tube voltage was almost equal to the charging voltage of the main condenser, and the peak current was about 15 kA. When the charging voltage was increased, the linear plasma formed, and the K-series characteristic x-ray intensities increased. The K-series lines were quite sharp and intense, and hardly any bremsstrahlung rays were detected. The x-ray pulse widths were approximately 700 ns, and the time-integrated x-ray intensity had a value of approximately 30 μC/kg at 1.0 m from the x-ray source with a charging voltage of 50 kV.

Keywords: Flash x-ray, weakly ionized linear plasma, K-series characteristic x-rays, monochromatic x-rays, x-ray divergence, rectilinear power

Laser-Generated & Other Lab. X-Ray & EUV Sources, Optics, Apps., ed. G. A. Kyrala, J.-C. J. Gauthier, C. A. MacDonald, A. M. Khounsary, Proceedings of SPIE Vol. 5196 (SPIE, Bellingham, WA, 2004) · 0277-786X/04/$15 · doi: 10.1117/12.506486